



A MLP Neural Network-Based Unified Intelligent Model for Predicting Short-Gap Breakdown Voltages in Air

Mounia Hendel^{1*}, Khadra Kessairi¹, Mostefa Brahami², Abderrezak Mansouri³

¹ Preparatory Classes Department, Higher School of Electrical and Energy Engineering of Oran, Oran 31000, Algeria

² Electrical department, Djilali Liabes University of Sidi Bel Abbes, Sidi Bel Abbès 22000, Algeria

³ Specialty department, Higher School of Electrical and Energy Engineering of Oran, Oran 31000, Algeria

Corresponding Author Email: hendel_mounia@esgee-oran.dz

Copyright: ©2024 The authors. This article is published by IETA and is licensed under the CC BY 4.0 license (<http://creativecommons.org/licenses/by/4.0/>).

<https://doi.org/10.18280/i2m.230304>

ABSTRACT

Received: 12 April 2024

Revised: 24 May 2024

Accepted: 4 June 2024

Available online: 21 June 2024

Keywords:

automatic regression, MLP neural network, short air gap, gradient backpropagation, breakdown voltage

The breakdown voltage characterizes the required voltage at which an electrical insulator will become a conductor of electricity. Measurements of short air gap discharge voltages are essential to guarantee safety, compliance and reliability in electrical energy transmission and transformation networks. After the implementation of three distinct neural models for three short air gap configurations prediction: Electrode-Sphere-Sphere-Earth (ESSE), Electrode-Sphere-plane (ESP), and Electrode-Symmetry-Sphere (ESS); the present research introduces an innovative compact and intelligent architecture to predict the breakdown voltages of any short air gap configuration (without having to resort to reconfiguring the system each time), based on a universal automatic multi-layer neural network (MLP) repressor. The unified architecture receives as input the radius, distance and indicator of the configuration and returns as output the predicted breakdown voltage. Our system has been validated on three configurations (with several internal diameter electrodes) and a fairly rich database (taken from the literature) with a Mean Square Error (MSE) of around 11.84%, which certify the yield of the methodology undertaken.

1. INTRODUCTION

Electrical insulation is an elementary characteristic when designing and implementing electrical systems, whose aim is to guarantee the separation of conductor or electrical constituents. This will prevent, any unwanted or unexpected contact that can lead to electric shocks, short circuits, or other unappreciated phenomena resulting from electricity circulation. The breakdown voltage represents the maximum voltage limit that an insulating material can withstand before suddenly losing its insulating properties and becoming conductive. This phenomenon's consequences are multiple: irreversible damage to the insulation compromising its insulation capacity, short circuits between conductors leading to electrical equipment malfunctions, etc. This damage can lead to a power supply interruption, which can have significant repercussions in critical areas [1-3].

Like any gaseous medium, atmospheric air is considered an insulator. In an aerial network, the air is subjected to sufficient electrical voltage. In the presence of impurities and severe atmospheric conditions, a current of electrically charged particles becomes possible through the medium partial ionization [4-6]. Consequently, the air becomes conductive, which leads to breakdown. Alternatives and models for estimating electrical breakdown voltages are in high demand for areas involving electrical insulation, more particularly, in energy transportation and distribution networks; The models allow, in fact, to predict with certainty the electrical equipment sizing, to develop efficient technologies for preventing

atmospheric discharges, and to accurately deduce safety distances.

The study of breakdown in air gaps has been the subject of several research in recent years. However, the airflow mechanism still needs to be fully understood. Methods for measuring breakdown voltage are subdivided into two approach categories: conventional methods (experimentally and theoretical) [7-10] and methods based on Artificial Intelligence (AI). Traditional methods of measuring breakdown voltage have certain disadvantages. On the one hand, these methods involve sophisticated equipment and require complex installations (such as special measuring chambers), thus making their implementation very expensive and limiting their accessibility and use. On the other hand, the results obtained are hazardous and of limited use due to the atmospheric conditions influence and the discharge energy influence on the samples studied. These drawbacks push the scientific community to intensify their research in order to propose more ingenious, efficient and economical breakdown measurement approaches. AI methods, inspired by living things' reasoning mechanisms, are seen as a critical solution due to the multitude of significant advantages they present. Indeed, AI promises to save time through the automation of the estimation process. AI ensures accurate, reliable results and reduces computing costs by eliminating expensive devices. Finally, AI has the particularity of learning from experience and adapting to situations never seen before, which makes it very suitable for the problem of approximating the electrical insulators' breakdown voltages, particularly air. With this in

mind, several ingenious research in the field of breakdown voltage estimation based on intelligent regression approaches have been proposed, including those based on neural networks [11-15], those based on Support Vector Regression (SVR) [16-20], those based on Support Vector Machine (SVM) [11, 21, 22], those based on fuzzy logic [23, 24] and those based on extremely randomized trees algorithm [11]. In what follows, we will detail some studies that are pretty similar to ours:

- Yang et al. and Yao et al. [16, 17] proposed an intelligent system based on SVR optimized by Cuckoo Search (CS) and weighted by grey relation analysis (CS- ω -SVR) in order to calculate the 50% breakdown voltage of the long rod-rod gap under different atmospheric conditions and different distances. The proposed method was validated on 70 samples. The authors selected two error indices to quantify the accuracy of the predicted results: mean absolute percentage error, which is on the order 8.8%, respectively. The researchers also highlighted that the proposed optimization algorithm was found to be more accurate than other algorithms such as GA and PSO.
- Kalenderli et al. [12] proposed a study to predict the breakdown voltage and gap types of a point-barrier air gap by training a Multi-Layer Perceptron neural network (MLP). The authors also present a comparison of the implemented method obtained results with those obtained by the methods of: maximum likelihood, graphical techniques and the least squares method. The results show that the breakdown voltages obtained by the MLP are practically identical to the reference values compared to the four other methods.
- Mokhnache and Boubakeur [15] implemented a Radial Basis Function (RBF) improved by the random optimization method (ROM) to predict the breakdown voltage in a barrier-point-plane air space for different voltage pulse forms (lightning pulse and switching pulse). In conclusion, the authors underline the method's effectiveness and even underline the possibility of extending their approach to the other parameters' prediction.
- The research by Qiu et al. [21] presents a new method for predicting breakdown voltages of typical air gaps (considering several configurations, namely, sphere-sphere, rod-plane, sphere-plane and sphere-plane-sphere), based on the Electric Field (EF) characteristics (in agreement with the results of finite element calculation) and an SVM (translating the regression problem into another dichotomous discrimination problem).
- Qiu et al. [22] presented a model for predicting the breakdown voltage of short air gaps (three configurations are considered in this study, namely, sphere-sphere, rod-plane, and rod-gaps between rods) based on the static EF distribution characteristics, an Orthogonal Design (OD) feature reduction approach and SVM. The obtained results showed a satisfactory correlation with the experimental data, with an average error percentage of around 3.9%.
- Yao et al. [14] proposed a new approach for determining the precise breakdown voltages of the rod-plane space and took into consideration two critical factors (temperature and humidity). The authors use an approach based on a regularization Invariant Risk Minimization Neural Network (IRM-NN), and they obtained an average error percentage of around 2.59%.

A thorough analysis of the intelligent systems proposed previously allowed us to raise the following limits: (1) Unlike

MLP, RBF is generally favorable for studies whose training sample numbers are quite limited; however, it is necessary to improve them by optimization techniques and vector quantification otherwise. (2) SVR remains favorable in both cases. Nevertheless, their rather complex mathematical foundation and the need to adjust their hyper parameters make their implementation very difficult and expensive in terms of implementation time. (3) The SVM use based on the translation of a regression problem to a classification problem is a bad idea because the obtained results will be non-precise and bounded in an interval. (4) Fuzzy logic is a compelling alternative. However, it remains based on the living beings' logical reasoning, which can make it ineffective in the face of unforeseen situations. In this study, we opted for using MLP because, on the one hand, we have a reasonably rich database which will allow us to train them well; and on the other hand, MLP-type neural networks offer a multitude of advantages, including: adaptability, non-linear data management, ability to extract characteristics from noisy data, robustness to noisy data, effectiveness for regression problems and performance improvement with the data quantity augmentation, etc.

Furthermore, the state of the art allowed us to conclude that despite the existence of a multitude of approaches to estimate the breakdown voltage of different air gap configurations and despite the existence of models which will enable switching between one configuration to another by taking only one configuration at a time. It isn't easy to find models that can guarantee the ability to easily adapt to additions of configurations (the possibility of extending the model) in a relatively simple way (natural, flexible and intuitive) without having to resort to neglecting configurations previously implemented in the same model. The only researches found are that of the studies [21, 22], which proposes a system that manages several configurations at the same time. All the same, this system remains primarily based on breakdown voltage estimation techniques based on mathematical and experimental calculation models (the disadvantages of which are cited above in the introduction); the SVM are only used to refine the tensions already obtained with precision. Furthermore, despite the good results obtained, the implemented systems remain quite complicated and require a fairly long execution time.

In this sense, the present study first presents a unique configuration based on MLP (in adequacy with existing models), with the aim of separately approaching the breakdown voltages of three distinct air gap configurations: Electrode-Sphere-Sphere-Earth (ESSE), Electrode-Sphere-plane (ESP), Electrode-Symetry-Sphere (ESS). Subsequently, the novelty of this research lies in the proposition of a new 100% intelligent unifier architecture is proposed to support all the air gap configurations studied. Thus, the proposed unified model has as first objective to propose a simple and flexible architecture 100% intelligent, which allows a fluid extension of the model to manage other configuration types. The model has as second objective to propose an efficient estimator with the speed and the precision of calculation, which will allow to consider an integration in real time/processes.

This paper is organized as follows: Section 2 will be devoted to the used database presentation. Section 3 will be dedicated to a brief description of the MLP mathematical foundation, followed by a well-established description of the proposed unified model. Section 4 will be reserved for the listing and discussion of the obtained results. Section 5 of this paper will serve as a conclusion.

2. THE USED DATABASE

Table 1. Training and estimation examples distribution according to each configuration

Configuration Type	Examples Numbers According to the Sphere Radius				Total examples number
	a=250 mm	a=125 mm	a=62.5 mm	a=31.25 mm	
ESSE	29	16	12	8	65
					Learning: 50.77%
ESP	30	22	15	-	67
					Learning: 50.76%
ESS	-	29	18	11	58
					Learning: 50.72%

We have a database made up of 190 examples taken from the research work of Donohoe et al. [25]. Three electrode configurations are considered in this study for the test and training samples construction:

- ESSE: containing 65 examples and four inter-electrode distances (a=250 mm, a=125 mm, a=62.5 mm and 31.25 mm);
- ESP: including 67 examples and three inter-electrode distances (a=250 mm, a=125 mm and a=62.5 mm);
- ESS: containing 58 examples and three inter-electrode distances (a=125 mm, a=62.5 mm and 31.25 mm).

The distribution of test and training sample distributions is presented in Table 1 and Figures 1-4 in accordance with the configurations considered. For each configuration and each diameter, the data sets were split into two: a training set and an estimation set.

Before splitting the global base, a centred/reduced normalization process (Eq. 1) was applied in order to keep the same distribution for all samples. The normalization is done separately by taking into consideration each configuration sample for the unique estimators, and the normalization is done on a global basis for the proposed hybrid estimator implementation.

$$\tilde{x}_{ij} = \frac{(x_{ij} - \bar{x}_j)}{\sigma_{xj}} \quad (1)$$

where, \bar{x}_j is the mean and σ_{xj} is the standard deviation.

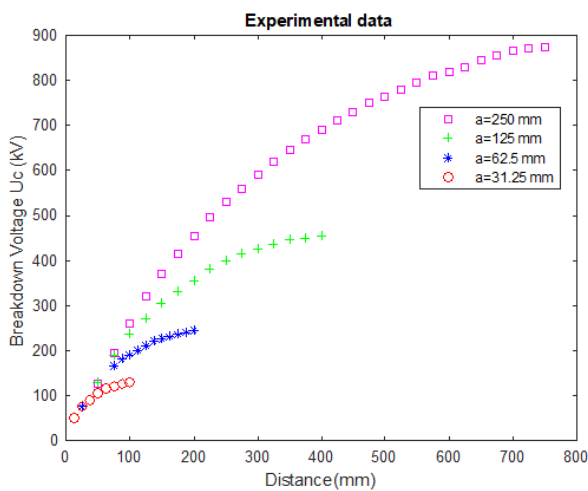


Figure 1. Experimental examples distribution (ESSE configuration)

We note that other normalization techniques have been tested, namely "Min-Max normalization" (Eq. 2) and "Log

transformation" (Eq. 3). The three normalization approaches were applied to the data set considered in this study, to obtain new normalized sets; the approximators performances were then evaluated based on each new set. For all configurations, the test results obtained with "centred/reduced normalization" reflected a significant reduction in the estimation error compared to other techniques.

$$x'_{ij} = \frac{x_{ij} - \min(x_j)}{\max(x_j) - \min(x_j)} \quad (2)$$

$$x'_{ij} = \log(x_{ij}) \quad (3)$$

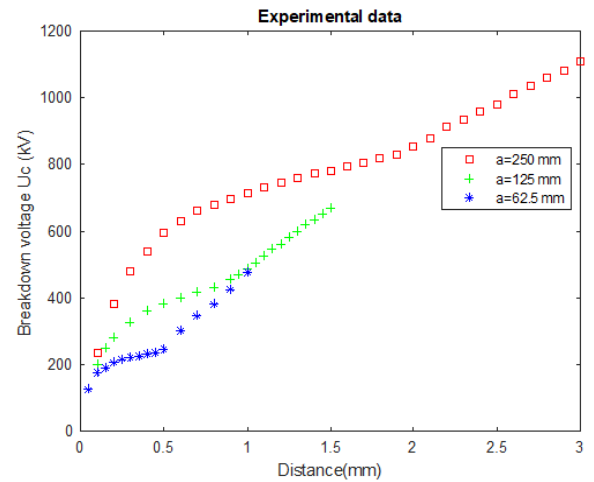


Figure 2. Experimental examples distribution (ESP configuration)

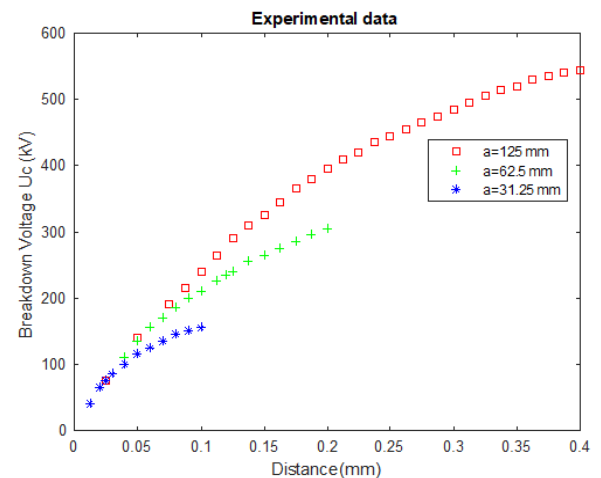


Figure 3. Experimental examples distribution (ESS configuration)

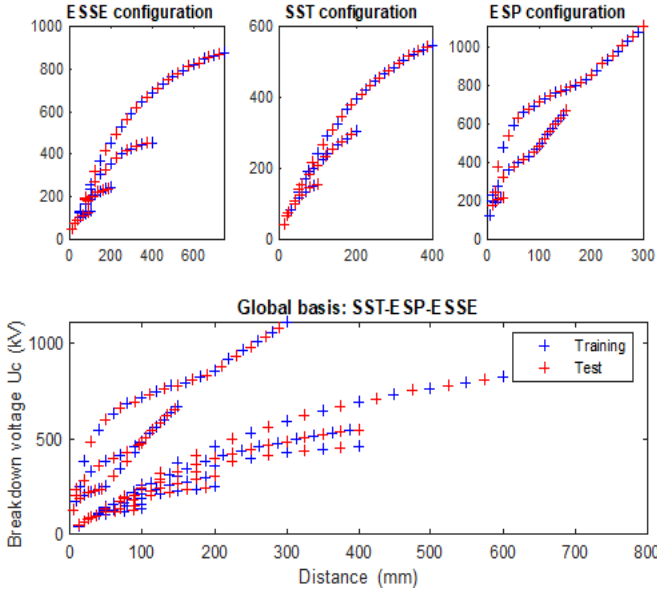


Figure 4. Training and estimation examples distribution (unique configuration)

3. THE PROPOSED MODELS IMPLEMENTATION

MLP is a supervised learning model with high computational capacity. Its structure consists of an “input layer”, an “output layer” (interpreted as the response of the network) and one or more intermediate layers called “hidden layers”. A neuron in the bottom layer can only be connected to neurons in subsequent layers. In this study, the MLP is considered for the breakdown voltages calculation in short air gap configurations; it is, in fact, a regression problem.

The regression model hyperparameters selection is a crucial and essential step for an intelligent mathematical model design, capable of behaving effectively in the face of test examples never before seen. For an MLP type approximator, the optimized parameters are those relating to: hidden layer number, the hidden layer neuron number, the activation functions, the metric chosen for the learning error evaluation and the learning algorithm.

- The hidden layer neuron number is usually proportional to the input vector size. Our test and training examples are samples that each has three parameters, therefore, a single hidden layer is sufficient to guarantee good prediction results (a higher number of hidden layers can cause the estimator overfitting).
- The hidden layer neurons number is fixed empirically by testing several configurations whose neurons number is included in the range (8-25); each configuration was repeated ten times due to the synaptic weights random initialization (at the beginning of training). The keeping configuration is the one that gives the best result (Table 2).
- As activation functions, we used a “Tansig-type” activation function for the hidden layer neurons and a “Purelin-type” activation function for the output layer neurons.
- The learning algorithm and the error evaluation metric used are respectively, the backpropagation learning rule and Mean Square Error (MSE); due to their effectiveness which has been proven in several applications.

3.1 Gradient back propagation algorithm

In the multilayer network structure, the gradient back propagation method is most frequently used to minimize the Mean Square Error (MSE) between the network output and the desired output. This algorithm back-propagates the error gradient from the output to the input. This operation is repeated until the difference between the network output and the desired output becomes acceptable (Figure 5).

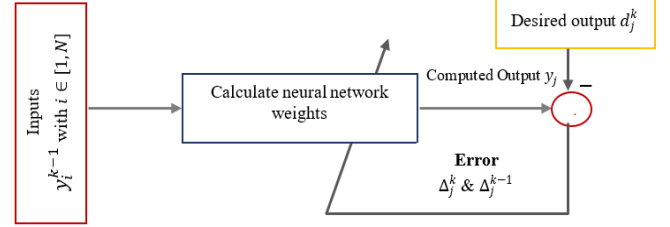


Figure 5. Synaptic weights modification in supervised learning

Learning by backpropagation is carried out in successive steps, which are described above [26, 27]:

- 1) The synaptic coefficients are initialized with small random values (NB: large values tend to cause the activation functions to become saturated).
- 2) Presentation of the characteristic vectors as input to the classifiers.
- 3) Iteratively calculate the neuron states in the following layers using Eq. (2).

$$y_j^k = f \left(\sum_{i=1}^N w_{ji}^k \cdot y_i^{k-1} \right) \quad (4)$$

with:

f : activation function.

N : neurons number in layer $k-1$.

k : current layer number.

y_j^k : output of neuron j from layer k .

w_{ji}^k : connection between neuron i of layer $k-1$ and neuron j of layer k .

y_i^{k-1} : output of neuron i from layer $k-1$.

- 4) Calculation of the error gradient made on neuron i in the output layer:

$$\Delta_j^k = 2f' \left(\sum_{i=1}^N w_{jk}^k \cdot y_j^{k-1} \right) \cdot (d_j^k - y_j^k) \quad (5)$$

with:

f' : the derivative of the function f .

d_j^k : the desired output for neuron i in layer k .

- 5) Back-propagated error gradients calculation from layer k to layer 1:

$$\Delta_j^{k-1} = 2f' \left(\sum_{i=1}^N w_{jk}^k \cdot y_j^{k-1} \right) \cdot \sum_{i=1}^N \Delta_j^k w_{ji}^k \quad (6)$$

- 6) Synaptic coefficients update:

$$w_{ji}^k(t+1) = w_{ji}^k(t) + \Delta_j^k \cdot y_j^k \quad (7)$$

with:
 Δ : is the gradient step.

Repeat all steps, except the first, each time for a new characteristic vector, until the stop test is activated.

3.2 MLP for a separate configuration breakdown voltage estimating

This sub-section will be devoted to presenting the methodology adopted to implement our unique intelligent estimators, each of which is responsible for interpolating the breakdown voltages of a single electrode geometry configuration. Each selected architecture is a three-layer configuration (Figure 6):

- An input layer: made up of two neurons, the first receiving the distance, and the second receiving the radius.
- A single hidden layer: the number of which is fixed empirically by testing several values and keeping the one that gave the best result (Table 2).
- An output layer is made up of a single neuron that returns the estimated breakdown voltage.

The MSE evaluation is shown in Figures 7-9. From the three figures, we can see a perfect convergence with quadratic errors, which are of the order of ESSE: 6.295, ESP: 6.966 and ESS: 2.0598. These findings prove the effectiveness of the unique configurations proposed.

3.3 MLP unified model

The goal of this section is to propose a compact architecture that makes it possible to address the problem in its entirety by supporting all three configurations (ESSE, ESP, and ESS). The training and testing data are the concatenation of the sets used to train and test the networks of the three configurations (ESSE, ESP and ESS) individually. The development of this unique network (see Figure 10) requires:

- There are three input neurons: one that receives the distance from which we want to estimate the breakdown voltage, one that receives the radius, and one that receives the configuration type (1 for SST, 2 for ESP, and 3 for ESS).
- One hidden layer whose neuron number was fixed empirically by testing several values and keeping the one that gave the best result (Table 3).
- A single output neuron that gives the estimated breakdown voltage.

The squared error during the iterations is schematized in Figure 11. We see a very satisfactory convergence (with an MSE of around 11.5835), which once again proves the effectiveness of the proposed configuration.

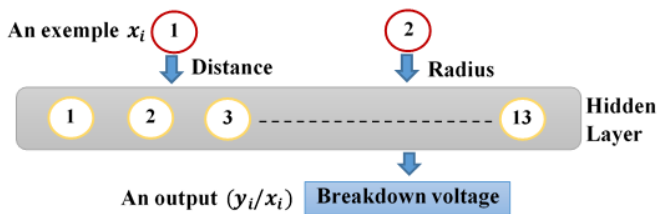


Figure 6. Graphical representation of the single model's configuration

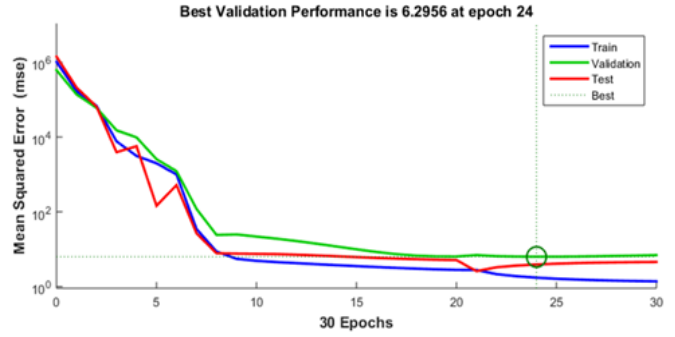


Figure 7. MSE error evolution during the iteration (ESSE configuration)

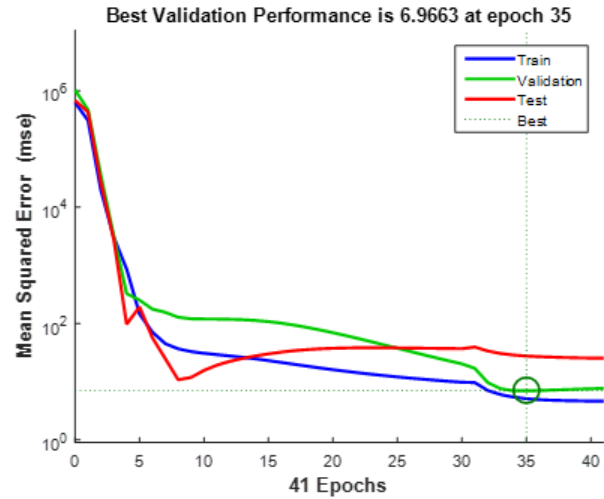


Figure 8. MSE error evolution during the iteration (ESP configuration)

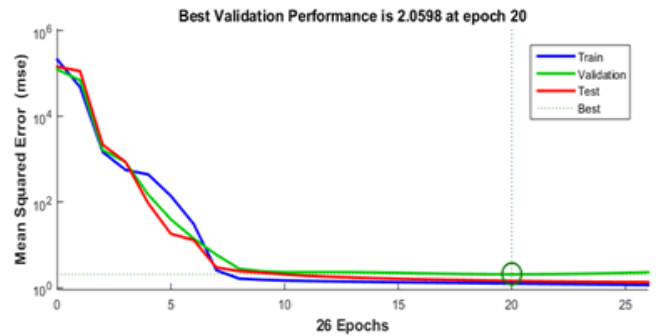


Figure 9. MSE error evolution during the iteration (ESS configuration)

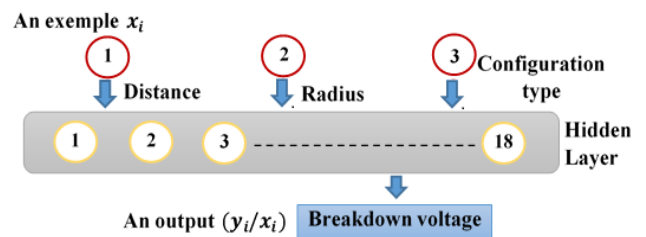


Figure 10. Graphical representation of the unique model configuration

Table 2. MSE evolution according to the hidden layer neurons number

Neurons Number	5	7	9	11	13	15	17	19	21	23	25	27	29
ESSE	33.20	37.19	19,88	11.65	6.29	8.64	9.76	22.18	25.23	16.15	32.23	33.31	34.86
ESP	29.85	35.10	18.85	12.72	6.96	9.66	10.62	26.84	23.24	17.55	33.41	31.47	35.85
ESS	5.92	3.78	2.96	4.42	2.05	3.57	4.65	3.01	4.30	3.59	5.61	5.10	6.66

Table 3. MSE evolution according to the hidden layer neurons number

Neurons Number	8	10	12	14	16	18	20	22	24	26
MSE	62.19	46.25	46.39	96.81	21.65	11.58	16.79	28.78	35.48	48.98

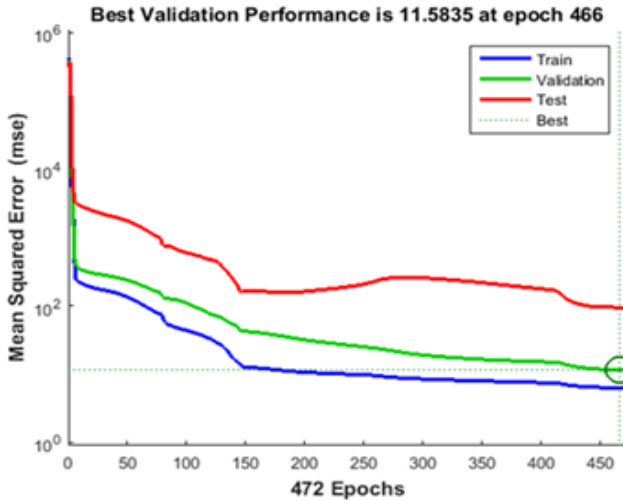


Figure 11. MSE error evolution during the iteration (unique configuration)

4. RESULTS AND DISCUSSION

This section presents the obtained results after learning our different unique models and the proposed global model.

4.1 Electrode-Sphere-Sphere-Earth (ESSE)

After the learning phase comes the test phase, from which the estimator performance is tested, Figure 12 illustrates the obtained results in the test phase. The outputs given by the network coincide in the majority of cases with the desired outputs with an MSE of 6.71%.

In order to properly view and analyse the obtained results, we list in Table 4 the obtained estimates and the estimation

error for each distance. We see that the testing errors for all the sphere radius are insignificant and almost zero. This underlines the undertaken approach effectiveness and also proves the efficient execution of the model training phase.

4.2 Electrode-Sphere-plane (ESP)

Once the network was trained, we presented it with all the experimental test data; the network responses are listed in Table 5 and Figure 13.

We notice from the obtained test results that the calculated output and the expected output are practically identical with an equal MSE to 7.15%. This confirms that the proposed network is well-trained and is able to behave effectively when faced with new examples.

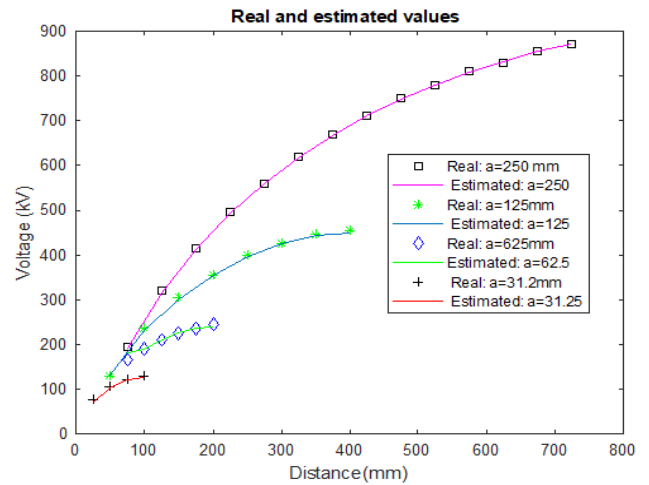


Figure 12. Obtained test results by the proposed architecture (ESSE configuration)

Table 4. Error in test (ESSE configuration)

Sphere Radius 250 mm														
Estimated output	193	317	416	490	558	622	675	711	747	780	805	832	856	871
Desired output	195	320	415	495	560	620	670	710	750	780	810	830	855	870
Error	2	3	-1	5	2	-2	-5	-1	3	0	5	-2	-1	-1
Sphere Radius 125 mm														
Estimated output	133	230	301	355	396	425	444							
Desired output	130	235	305	355	400	425	445							
Error	-3	5	4	0	4	0	1							
Sphere Radius 62.5 mm														
Estimated output	166	191	210	225	236	240								
Desired output	165	190	210	225	235	245								
Error	-1	-1	0	0	-1	5								
Sphere Radius 31.25 mm														
Estimated output	77	105	122	131										
Desired output	75	105	120	130										
Error	-2	0	-2	-1										

Table 5. Error in test (ESP configuration)

Sphere Radius 250 mm															
Estimated output	379	544	629	679	715	744	771	794	817	853	911	965	1014	1057	1109
Desired output	380	540	630	680	715	745	775	795	820	855	915	960	1010	1060	1110
Error	1	-4	1	1	0	1	4	1	3	2	4	-5	-4	3	1
Sphere Radius 125 mm															
Estimated output	247	330	380	413	457	489	526	563	600	635	672				
Desired output	250	325	380	415	455	485	525	560	600	635	670				
Error	3	-5	0	2	-2	-4	-1	-3	0	0	-2				
Sphere Radius 62.5 mm															
Estimated output	171	205	218	229	248	343	427								
Desired output	175	205	220	230	245	345	425								
Error	4	0	2	1	-3	2	-2								

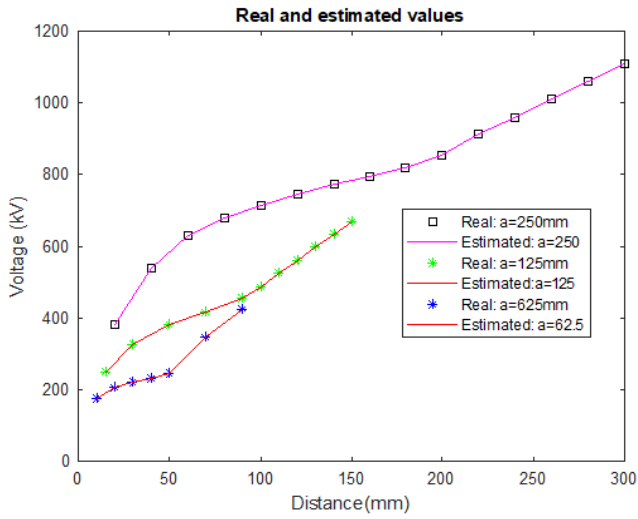


Figure 13. Obtained test results by the proposed architecture (ESP configuration)

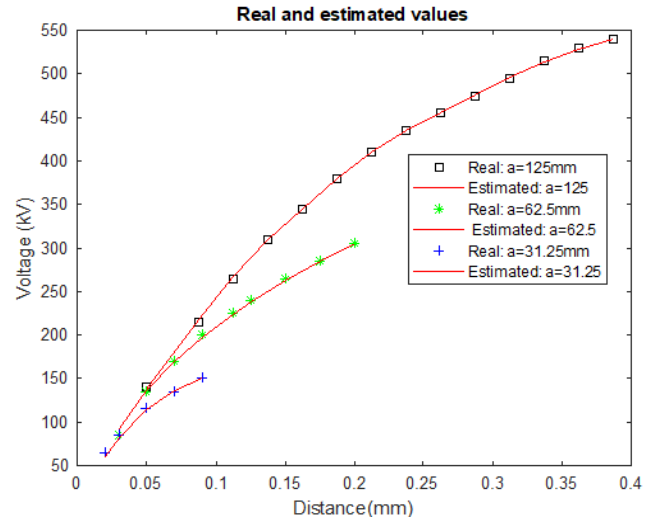


Figure 14. Obtained test results by the proposed architecture (ESS configuration)

Table 6. Error in test (ESS configuration)

Sphere Radius 125 mm														
Estimated output	137	218	265	307	345	379	409	435	459	479	497	513	527	540
Desired output	140	215	265	310	345	380	410	435	455	475	495	515	530	540
Error	3	-3	0	3	0	1	1	0	-4	-4	-2	2	3	0
Sphere Radius 62.5 mm														
Estimated output	88	133	171	201	227	241	265	285	305					
Desired output	85	135	170	200	225	240	265	285	305					
Error	-3	2	-1	-1	-2	-1	0	0	0					
Sphere Radius 31.25 mm														
Estimated output	63	85	115	134	152									
Desired output	65	85	115	135	150									
Error	2	0	0	1	-2									

4.3 Electrode-Symmetry-Sphere (ESS)

At the end of the learning phase of this new geometry configuration, the test examples were presented as input to the regression model; the breakdown voltages estimated by the network in the test phase are listed in Table 6 and Figure 14 (separately for each sphere radius).

The test results show that the calculated output and the expected output are practically identical with an MSE equal to 3.82%, this confirms that the proposed network is well-trained and can behave effectively when faced with new examples; and once again prove the effectiveness of: the two input choices, the adopted procedure to choose the hidden layer neuron numbers and the learning procedure.

4.4 Unified configuration

Once the network was trained, we tested it by first presenting the test data for each configuration individually (Figures 15-17) and then all the experimental data (Figure 18), the error representation is also shown in Figure 18. The obtained results reflect in the majority of cases, an estimated tension that coincide with the real values with an MSE of around of 11.84%.

In conclusion, we note that the proposed hybrid model, which is based mainly on a universal MLP-type estimator trained with the gradient back-propagation algorithm, effectively addresses the problem of estimating the breakdown voltage from the distance between electrodes; since, in all cases, the error between the actual breakdown voltage and the

estimated voltage does not exceed 10 KV. Theoretically these results are very encouraging; in the worst case an error of 10 KV for example, for a breakdown voltage of 380 KV is insignificant since the error only represents 2.65% of the overall percentage.

4.5 Comparative analysis

A comparative study is necessary to position this study in relation to the studies previously proposed in the literature. However, it is not apparent to favour one result or another; several parameters must be taken into consideration. So, for comparison, Table 7 below illustrates the results of some studies similar to ours from the point of view of the following: considered configuration type, concerned configuration number at the same time, air gap type, and MSE error.

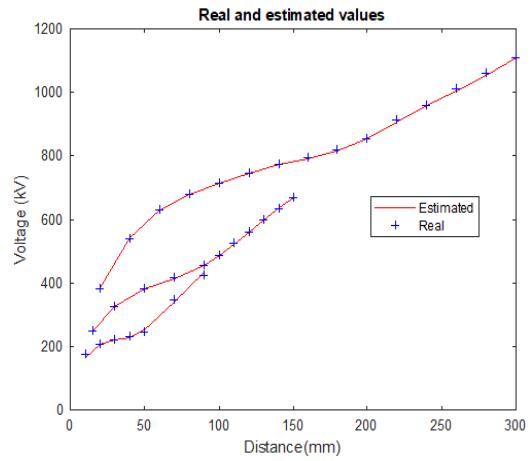


Figure 16. Obtained test results by the proposed unified architecture (ESP configuration)

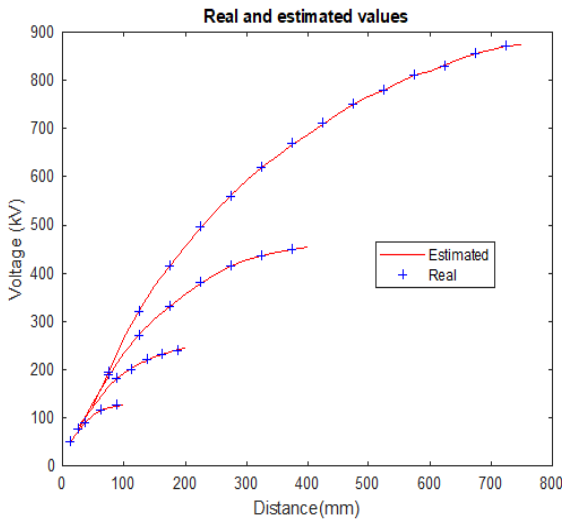


Figure 15. Obtained test results by the proposed unified architecture (ESSE configuration)

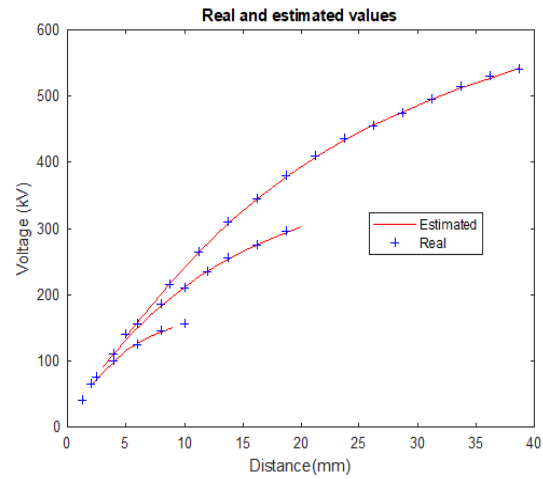


Figure 17. Obtained test results by the proposed unified architecture (ESS configuration)

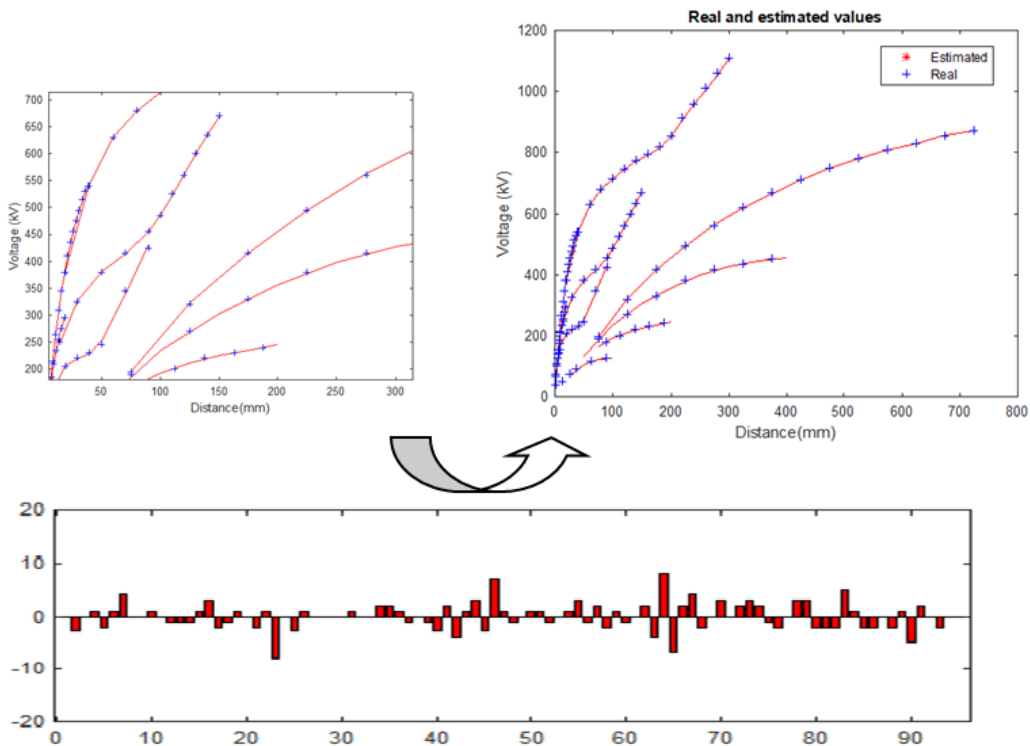


Figure 18. Global obtained test results by the proposed unified architecture (for all configurations)

Table 7. Comparative analysis

Study	Configuration Type	Configuration Number	Air Gap Type	Samples Number	MSE Error
CS- ω -SVR [16, 17]	rod-rod	One configuration at a time	Long gap	14	8.8
MLP [12]	point-barrier	One configuration at a time	Not mentioned	Not mentioned	9.91
RBF-ROM [15]	barrier-point-plane	One configuration at a time	Long gap	≈ 50	5.8
EF-SVM [21]	sphere-sphere, rod-plane, sphere-plane and sphere-plane-sphere	four configurations at a time	Short gap	25	4.12
EF-OD-SVM [22]	sphere-sphere, rod-plane and rod-gaps between rods	three configurations at a time	Short gap	99	6.86
IRM-NN [14]	rod-plane space	One configuration at a time	Long air gap	Not mentioned	2.59
Current study	ESSE configuration	One configuration at a time	Short gap	65	6.71
	ESP configuration			67	7.15
	ESS configuration	three configurations at a time		58	3.82
	Unified model			190	11.84

From the table, we can see that the results obtained with the proposed approach are comparable and, in some cases, surpass other studies [12, 16, 17]. Indeed:

- The study [15] considers only one configuration at a time and exposes lower MSE rates compared to our approach; however, the authors use a minimal test sample number. In addition, our study treats all the diameters for each configuration at the same time, which adds a certain complexity degree to the regression task, unlike other research. Finally, the study considers a long air gap type, which facilitates the estimating breakdown task, unlike the fairly small inter-electrode distances.
- As we have already mentioned, the studies [21, 22] remain the only studies that consider several configurations simultaneously. Our results are comparable to theirs, which present slightly basic MSE. But once again, our approach was validated on an example set twice as large as the study [22] and four times as large as the study [21]. We also recall that these two studies are mainly based on traditional approaches (the disadvantages of which were discussed in the introduction section). AI approaches were used to validate the obtained results, and they were based on translating a regression problem into a classification problem (much less precise and reliable).

All of these findings justify the proposed approach's effectiveness and validity. It significantly simplifies the task of estimating breakdown voltages, thus avoiding unforeseeable accidents that could be caused in electrical networks.

5. CONCLUSIONS

Through this research, a new unified intelligent model for predicting short-gap breakdown voltages based on the MLP neural network is proposed. To do this, we proceeded in a progressive manner:

- We first proposed specific automatic networks to estimate breakdown voltages separately for each of the following three configurations: ESSE, ESP and ESS.
- We have introduced a global estimator based on an MLP, able to support all configurations, thus allowing an integrated approach for the breakdown voltage estimation.
- We also proposed a learning process to determine the neuron's numbers in the hidden layer for the selected configurations, which contributes to minimize the MSE as much as possible and optimizes the networks

estimation.

The obtained estimates and desired outputs are approximately identical in all cases, and the error is practically zero for all the geometries considered in this study (the unified architecture and the specific architectures). Comparisons between the obtained results with different approaches reported in the literature [12, 14-17, 21, 22] also indicate the effectiveness, validity and significant impact of the proposed unified model despite its simplicity.

These results are very encouraging and confirm the effectiveness of the adopted approach and its potential to improve the breakdown voltage estimation performance in areas involving electrical insulation, bringing precision and safety in the electrical equipment sizing. However, this research could be improved by considering the following future work: studying the environmental factors (temperature, humidity, pressure) effect, testing other geometries type, and implementing other automatic regressors type and provide the merger for greater credibility.

ACKNOWLEDGMENT

This work was supported by the PRFU-C00L07EP31022010001 project and the General Directorate for Scientific Research and Technological Development (DGRSDT).

REFERENCES

- [1] Kumar, D., Alam, M., Zou, P.X., Sanjayan, J.G., Memon, R.A. (2020). Comparative analysis of building insulation material properties and performance. *Renewable and Sustainable Energy Reviews*, 131: 110038. <https://doi.org/10.1016/j.rser.2020.110038>
- [2] An, Y.Z., Yin, K.Q., Huang, T., Hu, Y.C., Ma, C.H., Yang, M.H., An, B.C., Chen, D. (2022). Study on the insulation performance of SF6 gas under different environmental factors. *Frontiers in Physics*, 10: 820036. <https://doi.org/10.3389/fphy.2022.820036>
- [3] You, T., Dong, X., Zhou, W., Qiu, R., Hou, H., Luo, Y. (2022). Research and analysis of insulating gas in unified test conditions. *ACS Omega*, 7(11): 9221-9228. <https://doi.org/10.1021/acsomega.1c05760>
- [4] An, Y.Z., Su, M.H., Hu, Y.C., Hu, S.M., Huang, T., He, B.N., Yang, M.H., Yin, K.Q., Lin, Y.T. (2022). The

- influence of humidity on electron transport parameters and insulation performance of air. *Frontiers in Energy Research*, 9: 806595. <https://doi.org/10.3389/fenrg.2021.806595>
- [5] Li, B., Li, X., Fu, M., Zhuo, R., Wang, D. (2018). Effect of humidity on dielectric breakdown properties of air considering ion kinetics. *Journal of Physics D: Applied Physics*, 51(37): 375201. <https://doi.org/10.1088/1361-6463/aad5b9>
- [6] Ji, Y., Giangrande, P., Zhao, W., Madonna, V., Zhang, H., Li, J., Galea, M. (2023). Investigation on combined effect of humidity–temperature on partial discharge through dielectric performance evaluation. *IET Science, Measurement & Technology*, 17(1): 37-46. <https://doi.org/10.1049/smt2.12128>
- [7] Taniguchi, S., Okabe, S., Asakawa, A., Shindo, T. (2008). Flashover characteristics of long air gaps with negative switching impulses. *IEEE Transactions on Dielectrics and Electrical Insulation*, 15(2): 399-406. <https://doi.org/10.1109/TDEI.2008.4483458>
- [8] Wang, Y., Wen, X., Lan, L., An, Y., Dai, M., Gu, D., Li, Z. (2014). Breakdown characteristics of long air gap with negative polarity switching impulse. *IEEE Transactions on Dielectrics and Electrical Insulation*, 21(2): 603-611. <https://doi.org/10.1109/TDEI.2013.003627>
- [9] Fofana, I., Beroual, A., Rakotonandrasana, J.H. (2013). Application of dynamic models to predict switching impulse withstand voltages of long air gaps. *IEEE Transactions on Dielectrics and Electrical Insulation*, 20(1): 89-97. <https://doi.org/10.1109/TDEI.2013.6451345>
- [10] Qin, J., Pasko, V.P. (2014). On the propagation of streamers in electrical discharges. *Journal of Physics D: Applied Physics*, 47(43): 435202. <https://doi.org/10.1088/0022-3727/47/43/435202>
- [11] Yang, B., Ding, Y., Lu, Z., Yao, X., Lei, T., Su, Y. (2021). Intelligent computing of positive switching impulse breakdown voltage of rod-plane air gap based on extremely randomized trees algorithm. *Electrical Engineering*, 103(6): 3177-3187. <https://doi.org/10.1007/s00202-021-01307-4>
- [12] Kalenderli, Ö., Bolat, S., Ismailoglu, H. (2003). Determination of critical impulse breakdown voltage by artificial neural network. In *Third International Conference on Electrical and Electronics Engineering*, Bursa, Turkey, <https://www.researchgate.net/publication/239920261>.
- [13] Qiu, Z., Wu, Z., Song, Y. (2023). Sphere gap breakdown voltage prediction based on ISSA optimized BP neural network and effective electric field feature set. *IEEE Transactions on Electrical and Electronic Engineering*, 18(4): 506-514. <https://doi.org/10.1002/tee.23750>
- [14] Yao, X., Su, Y., Yang, B., Ma, X., Ding, Y. (2023). Prediction of discharge voltage for rod-plane gap based on regularized IRM-NN and its generalization analysis. In *Proceedings of the 2023 7th International Conference on Computing and Data Analysis*, Guiyang, China, pp. 75-78. <https://doi.org/10.1145/3629264.3629275>
- [15] Mokhnache, L., Boubakeur, A. (2001). Prediction of the breakdown voltage in a point-barrier-plane air gap using neural networks. In *2001 Annual Report Conference on Electrical Insulation and Dielectric Phenomena (Cat. No. 01CH37225)*, Kitchener, ON, Canada, pp. 369-372. <https://doi.org/10.1109/CEIDP.2001.963559>
- [16] Yang, B.X., Yao, X.Y., Su, Y., Ding, Y.J. (2022). Intelligent computing and analysis of breakdown voltage of rod-rod long air gap. *Rural Electrification*, (10): 20-25. <http://doi.org/10.13882/j.cnki.ncdqh.2022.10.004>
- [17] Yao, X., Yang, B., Geng, J., Su, Y., Yu, H., Yang, G., Wang, X. (2022). Intelligent computing and analysis of breakdown voltage of rod-rod long air gap. *Journal of Physics: Conference Series*, 2215(1): 012011. <https://doi.org/10.1007/s00202-021-01307-4>
- [18] Qiu, Z., Ruan, J., Jin, Q., Wang, X., Shu, S. (2019). Discharge voltage prediction of UHV AC transmission line–tower air gaps by a machine learning model. *The Journal of Engineering*, 2019(16): 3140-3144. <https://doi.org/10.1049/joe.2018.8486>
- [19] Qiu, Z., Zhang, L., Liu, Y., Liu, J., Hou, H., Zhu, X. (2021). Electrostatic field feature selection technique for breakdown voltage prediction of sphere gaps using support vector regression. *IEEE Transactions on Magnetics*, 57(6): 1-4. <https://doi.org/10.1049/joe.2018.8486>
- [20] Ding, Y., Zhao, S., Yang, B., Yao, X., Ding, Y., Lu, Z. (2023). Breakdown characteristics and voltage calculations of large-size sphere-plane long air gaps. *Electrical Engineering*, 105(6): 4469-4479. <https://doi.org/10.1007/s00202-023-01952-x>
- [21] Qiu, Z., Ruan, J., Huang, D., Pu, Z., Shu, S. (2015). A prediction method for breakdown voltage of typical air gaps based on electric field features and support vector machine. *IEEE Transactions on Dielectrics and Electrical Insulation*, 22(4): 2125-2135. <https://doi.org/10.1109/TDEI.2015.004887>
- [22] Qiu, Z., Ruan, J., Huang, D., Wei, M., Tang, L., Huang, C., Xu, W., Shu, S. (2016). Hybrid prediction of the power frequency breakdown voltage of short air gaps based on orthogonal design and support vector machine. *IEEE Transactions on Dielectrics and Electrical Insulation*, 23(2): 795-805. <https://doi.org/10.1109/TDEI.2015.005398>
- [23] Rouini, A., Derbel, N., Hafaiifa, A., Kouzou, A. (2018). New approach for prediction the DC breakdown voltage using fuzzy logic controller. *Diagnostyka*, 19(3): 55-62. <https://doi.org/10.29354/diag/92294>
- [24] Mohanty, S., Ghosh, S. (2011). Modeling of the breakdown voltage of solid insulating materials using fuzzy logic techniques. In *2011 Annual Report Conference on Electrical Insulation and Dielectric Phenomena*, Cancun, Mexico, pp. 530-533. <https://doi.org/10.1109/CEIDP.2011.6232711>
- [25] Donohoe, J.P., Jiang, M.Y., Thompson, J.F., Miller, D.B. (1993). Computational simulation of electric fields surrounding power transmission and distribution lines. *The Applied Computational Electromagnetics Society Journal*, 8(2): 4-16.
- [26] Du, K., Hennigen, L.T., Stoehr, N., Warstadt, A., Cotterell, R. (2023). Generalizing backpropagation for gradient-based interpretability. *arXiv preprint arXiv:2307.03056*. <https://doi.org/10.48550/arXiv.2307.03056>
- [27] Wunderlich, T.C., Pehle, C. (2021). Event-based backpropagation can compute exact gradients for spiking neural networks. *Scientific Reports*, 11(1): 12829. <https://doi.org/10.1038/s41598-021-91786-z>

NOMENCLATURE

a	Radius
f	Activation function
N	Neurons number in layer $k - 1$
k	Current layer number
y_j^k	Output of neuron j from layer k
w_{ji}^k	Connection between neuron i of layer $k - 1$ and neuron j of layer k
y_i^{k-1}	Output of neuron i from layer $k - 1$
f'	The derivative of the function f
d_j^k	The desired output for neuron i in layer k
\bar{x}_j	The mean
\widetilde{x}_{ij}	Normalized parameter

Greek symbols

Δ	The gradient step
----------	-------------------

σ_{xj} The standard deviation

Subscripts

ESSE	Electrode-Sphere-Sphere-Earth
ESP	Electrode-Sphere-plane
ESS	Electrode-Symmetry-Sphere
MLP	Multi-Layer Perceptron neural network
MSE	Mean Square Error
AI	Artificial Intelligence
SVR	Support Vector Regression
SVM	Support Vector Machine
CS	Cuckoo Search
RBF	Radial Basis Function
ROM	Random Optimization Method
EF	Electric Field
OD	Orthogonal Design
IRM-NN	Invariant Risk Minimization Neural Network